Analysis of Vertical Strip wound Fault-Tolerant Permanent Magnet Synchronous Machines

Puvan Arumugam, Tahar Hamiti, Christopher Brunson and Chris Gerada

Abstract— **This paper investigates the behavior of a vector-controlled, fault-tolerant, permanent magnet motor drive system adopting a vertically placed strip winding (VSW) which can limit inter-turn short-circuit (SC) fault current to its rated value regardless of the position in the slot containing the shorted turns. The drives' dynamic behavior is simulated using a per-phase equivalent circuit model with the winding inductances and resistances analytical calculated based on the machine geometry and fault location. A simplified thermal model is also grafted into the system model to effectively simulate the dynamic behavior of the machine during healthy, inter-turn SC fault and post-fault controlled scenarios. The SC fault current limiting capability, the additional losses and thermal behavior of the winding are studied and compared with conventional winding adopting round conductors winding (RCW). The proposed winding design is verified with Finite Element (FE) analysis and then validated experimentally. Results show that the VSW inherently limits the SC current, reduces its dependence on the position of the fault within the slot but results in an increase in AC losses.**

Index Terms— **Copper loss, Concentrated windings, Fault-tolerant, Permanent magnet, Short-circuit, Slot-leakage**

I. INTRODUCTION

Permanent magnet synchronous machines (PMSM) [1-4] are increasingly being used in safety critical applications such as in aircraft and other transportation systems. In such applications the necessary system reliability level can be reached by designing for fault tolerance and hence avoiding replicating the complete drive system [5]. This generally leads to a reduced overall system weight and component count.

A typical fault-tolerant Permanent Magnet Synchronous Machine (FT-PMSM) drive topology includes a number of design features [5-13] to enable a level of operation when faults [3, 13-17] ensue. Although such a machine drive topology, if appropriately designed, can potentially tolerate converter failures, winding open circuit failures and terminal

The authors are all with the Power Electronics, Machines and Control Group, Faculty of Engineering, the University of Nottingham, University Park, Nottingham, NG7 2RD. UK.
  Puvan Arumugam (e-mail: puvan.arumugam@nottingham.ac.uk)
  Tahar Hamiti (e-mail: mohand.hamiti@nottingham.ac.uk)
  Christopher Brunson (e-mail: eexcmb@nottingham.ac.uk)
  Chris Gerada (e-mail: chris.gerada@nottingham.ac.uk)

SC failures, a winding inter-turn (a single turn) SC fault remains problematic [6]. If an inter-turn SC fault is left undetected and no compensation techniques are applied, the resulting current of the inter-turn SC fault is likely to be excessively high and can lead to catastrophic failures.
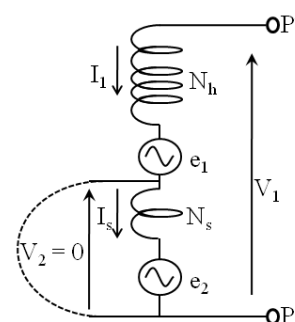

Fig.1.   Equivalent circuit of a phase winding of FT-PMSM under inter-turn short-circuit condition

Fig.1 shows a representative illustration of a one turn SC fault in a FT-PMSM, where, the phase winding is fed by a voltage source V_1. It is worth noting that there is a naturally strong mutual coupling (L_m) between a N_s shorted turn and the N_h remaining turns since both windings are located in the same slot. From Fig.1 it can clearly be seen that the magnitude of SC current (I_s) depends on induced emf (e_2) in the shorted turn due to the PM' flux at electrical speed ω, the supply current I_1, mutual coupling L_m and impedance (includes resistance R_s and inductance L_s) of the shorted turn as in equation (1) [6].

$$I_s = -\frac{e_2(\omega)}{R_s + j\omega L_s} - \frac{j\omega L_m}{R_s + j\omega L_s}I_1(\omega) \tag{1}$$

The main issue with turn-turn faults in safety-critical applications stems from the fact that even though the phase winding may be disconnected, the turn-turn SC fault current persists if rotation is maintained. Different researchers have dealt with this issue in different ways. These can be divided in five groups. One methodology is to apply a terminal short circuit to either the faulted phase, if each of the machine's phases is supplied separately [18] or else a balanced short to all the phases if the machine is fed through a single converter [19]. The underlying principle in these methods is that the

MMF is balanced in the internally shorted turn against the remaining winding which in-turn limits the fault current. The main benefit of this methodology is simplicity, however it is often very difficult to limit the current to rated if a single turn occurs. The second method is to apply a controlled current to the remaining healthy turns to minimise the total flux linkage of the shorted turn [20]. This is method requires a more complex control system and a considerably oversized converter to handle such operation. A third methodology which has been proposed but difficult to guarantee is to rely on a SC turning into an open circuit fault [21] by use of special wire. The last two methodologies are based on eliminating the faulted turns flux linkage either through a form of a mechanical actuation of the rotor/magnets to minimise flux linkage [22] or else by using a third winding to divert/short the magnet flux through a path which does not link with the faulted turn [23]. These methods are often not used due to the added complexity.

This paper is set around the first concept for limiting SC faults. The main difference is that by using the VSW the machine can be designed so that the any single faulted turn's current is always limited to that below rated [6]. It is a crucial advantage over RCW since the single turn fault' current of RCW is highly position dependent and significantly larger than rated when the fault located closer to slot opening region [6].

In the early studies [24-30], the dynamic behavior of RCW wound PMSM under healthy, faulty and post-fault control operating conditions have been investigated in both FE coupled dynamic models [31] and lumped-parameter dynamic model based on parameters calculated with FE [28]. However, in these early studies the influence of the location and geometry of the faulty winding on the fault behavior are not considered. Particularly, a detailed analysis of the effects of the VSW type of winding structure on the drive system operation was not presented before.

In this paper the electromagnetic and thermal analysis of VSW wound FT-PMSM is investigated under healthy, faulty with inter-turn SC and post-fault controlled operation based on parameters predicted analytically [6]. A dual three-phase winding arrangement [8, 32] is adopted in the FT-PMSM in order to achieve redundancy with the required level of reliability. This dual three-phase FT-PMSM model is developed in Simulink and integrated within the drive system model. An analytical model developed in [6] is integrated into a dynamic model of the FT-PMSM to estimate the dynamic model parameters under both healthy and faulty conditions. In addition, a simplified thermal model is included to effectively model the dynamic thermal behavior of the machine during inter-turn SC faults and post-fault controlled scenarios. The VSW winding design is verified with FE and then validated experimentally. In addition, the SC fault current limiting capability, loss and thermal behavior are studied and compared with a more conventional RCW structure. Results show that even though the VSW inherently limits the SC current and reduces the fault position dependency, the proximity losses in such a winding can be an issue at relatively high frequency operation. However these losses can be reduced to the level of losses in RCW by adequate design.

II. ANALYTICAL CALCULATION OF WINDING PARAMETERS

From Fig.1, as can be seen that during an inter-turn SC fault, the healthy and the shorted turns behave as two separate circuits which are magnetically coupled, but electrically isolated [7]. As a result, it changes the winding parameters: inductances, resistances and back- EMF. From (1), it can be seen that the induced current in the shorted turn can be evaluated once the inductances and resistances are determined. Whilst the dc resistances (neglecting skin and proximity effects) are independent of the shorted turns' position in the slot, the inductances are strongly position-dependant; hence an analytical method able to estimate these vales is adopted based on the slot-leakage flux estimation.

The flux associated with the winding under SC fault is represented as shown in Fig.2. Several assumptions have been made: the slot has a rectangular shape, the magnetic material has infinite permeability and VSW is placed vertically and uniformly in the slot. Under fault conditions, due to the relatively high induced SC current; it was assumed that the flux lines across the slot are parallel to the conductors, as illustrated in Fig.2.
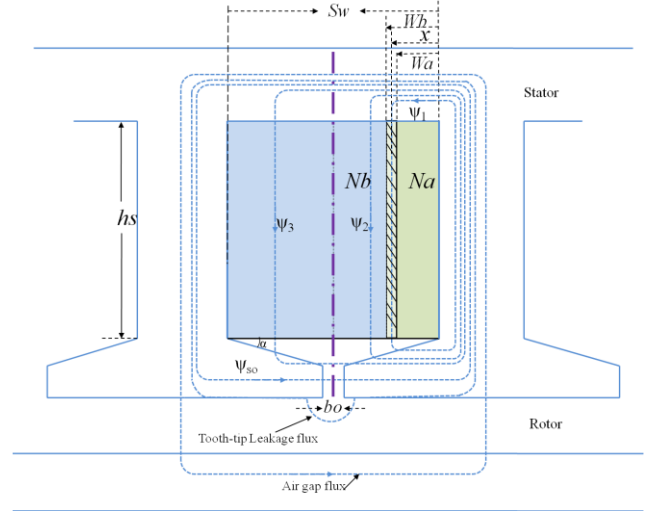

Fig.2. Flux representation used in the modeling of VSW

The shorted turn N_s is located in between the healthy turns N_a and N_b. The slot-leakage fluxes associated with shorted turn are Ψ_{so}, Ψ_1, Ψ_2 and Ψ_3. W_a and W_b are widths with respect to the varying position (x) of the N_s turn and other parameters are explained in Fig.2. Thus, the slot-leakage flux Ψ_1 is evaluated by integrating the flux density over the corresponding area as previously to be [6]

$$\Psi_1 = \int_{W_a}^{W_b} \mu_o \, l_{stk} \, I \left(\frac{N}{S_w} \right)^2 \left[\frac{(x - W_a)^2}{h_s + x \tan(\alpha)} \right] d\,x \qquad (2)$$

where, I represents the total current in the phase winding and l_{stk} is axial length of the machine. In similar way, the slot-leakage fluxes Ψ_{so}, Ψ_2 and Ψ_3 and main airgap, tooth-tip leakage flux can be evaluated. Hence the inductance is obtained by evaluating associated total flux for a unit current. The detailed evaluation of inductance can be found in [6].

III. DRIVE SYSTEM MODELING UNDER AN INTER-TURN SC FAULT

Analysis is carried out on a dual three-phase, 12 slots and 14 poles concentrated wound FT-PMSM (Fig.3). This dual three-phase arrangement is well known as a modular solution and investigated in [19, 32]. This solution has two separate three phase windings, A_1-B_1-C_1 and A_2-B_2-C_2, each supplied by a separate converter as shown in Fig.3. Thus, the VA rating of the converter corresponds to half the motor VA rating during normal operation. In the event of a failure of one of the dual three phase windings or corresponding converter, the respective unit is disconnected or short–circuited and the machine can then be operated with the remaining healthy unit. The loss of output power can be compensated by increasing current loading. It goes without saying that the machine and the converter have to be overrated at the design stage to handle the required current loading in the event of failure.
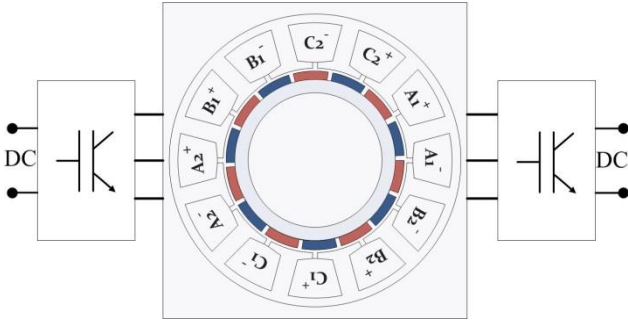

Fig.3. Representation of dual three phase drive

In the modeling of the dual three-phase machine, the governing dynamic equations are separated into the following three parts: electrical equations, mechanical equations and thermal equations.

1) Electrical equations
Neglecting magnetic saturation, the dual three phase (2 sets of star connected 3-phase windings fed separately by two 3-phase voltage source inverters) FT-PMSM drive is modeled in the stationary frame using the well-known governing dynamic equations as follows:

Machine 1:

$$V_{A_1B_1C_1} = I_{A_1B_1C_1} \; R_p + L_p \frac{d}{dt} I_{A_1B_1C_1} + e_{A_1B_1C_1}$$

$$\begin{cases} V_{A_1B_1C_1} = \begin{bmatrix} V_{A_1} \; V_{B_1} \; V_{C_1} \end{bmatrix}^T \\ I_{A_1B_1C_1} = \begin{bmatrix} I_{A_1} \; I_{B_1} \; I_{C_1} \end{bmatrix}^T \\ e_{A_1B_1C_1} = \begin{bmatrix} e_{A_1} \; e_{B_1} \; e_{C_1} \end{bmatrix}^T \end{cases} \quad (3)$$

Machine 2:

Henceforth we assume that machine 1 is healthy while an inter-turn SC fault occurs in machine 2. By substituting equation (1) into (3), with the corresponding index, a turn to turn fault is introduced in the system. The resistance, inductances and induced EMF are calculated based on the location and number of short-circuited turns.

$$V_{A_2B_2C_2f} = I_{A_2B_2C_2f} \; R_{A_2B_2C_2f} + L_{A_2B_2C_2f} \frac{d}{dt} I_{A_2B_2C_2f} + e_{A_2B_2C_2f}$$

$$\begin{cases} V_{A_2B_2C_2f} = \begin{bmatrix} V_{A_2} \; V_{B_2} \; V_{C_2} \; V_f \end{bmatrix}^T \\ I_{A_2B_2C_2f} = \begin{bmatrix} I_{A_2} \; I_{B_2} \; I_{C_2} \; I_f \end{bmatrix}^T \\ e_{A_2B_2C_2f} = \begin{bmatrix} e_{A_2} \; e_{B_2} \; e_{C_2} \; e_f \end{bmatrix}^T \end{cases} \quad (4)$$

where,
- R_p is phase resistance;
- L_p is the phase inductance;
- V, I and e are respectively the voltage, the current and the back-EMF of phases A_p, B_p and C_p;
- p = 1, 2 is the 3-phase winding set index.

It is worth noting that the coupling between the phases and also between machine 1 and 2 is neglected since the windings are concentrically wound around the teeth so as to be physically, thermally and magnetically decoupled. However, the mutual inductance between the shorted turns and the remaining turns of the faulty phase are accounted for as in the expressions below.

$$R_{A_2B_2C_2f} = \begin{bmatrix} R_p & 0 & 0 & 0 \\ 0 & R_p & 0 & 0 \\ 0 & 0 & R_h & 0 \\ 0 & 0 & 0 & R_s \end{bmatrix} \quad (5)$$

$$L_{A_2B_2C_2f} = \begin{bmatrix} L_p & 0 & 0 & 0 \\ 0 & L_p & 0 & 0 \\ 0 & 0 & L_h & L_m \\ 0 & 0 & L_m & L_s \end{bmatrix} \tag{6}$$

2) Mechanical equations

$$T_e = T_L + K_f\, \omega_m + J\, \frac{d\omega_m}{dt} \tag{7}$$

$$\theta_e = \int \frac{P}{2}\, \omega_m\, dt \tag{8}$$

where K_f represents the viscous friction coefficient; J is inertia; ω_m is the mechanical speed; θ_e is the electrical speed and T_L and T_e are the load and the electromagnetic torque respectively.

3) Thermal model

Before applying any post-fault remedial action the resulting SC current from a single turn SC can be much higher than the rated current and thus the temperature of the shorted turns can rise rapidly [33] thus having a significant effect on the turns' resistance and consequently on their impedance, especially when the number of short-circuited is small with the worst case scenario being a single turn fault. To assess this temperature rise a simplified thermal model is adopted. This makes a basic assumption that during the fault all the losses generated by the shorted turns go towards increasing the shorted turn's temperature. It is thus assumed that there is no heat transfer from the shorted turns to the surrounding adjacent turns and the magnetic material. This represents the worst-case scenario. Hence, the simplified thermal model can be expressed as follows:

$$T = \int_{t_0}^{t_1} \frac{I_s^2\, R_{new}}{m c_p}\, dt \tag{9}$$

where,

$$R_{new} = R_s\, (1 + \alpha_1\, (T - T_i)) \tag{10}$$

where R_s is the initial resistance at the operating speed of the machine; T_i is the initial temperature of the shorted turns which is assumed equal to room temperature (20° C); m is the mass of the shorted turns; α_t is the temperature coefficient of resistivity and C_p is the specific thermal heat capacity of copper.
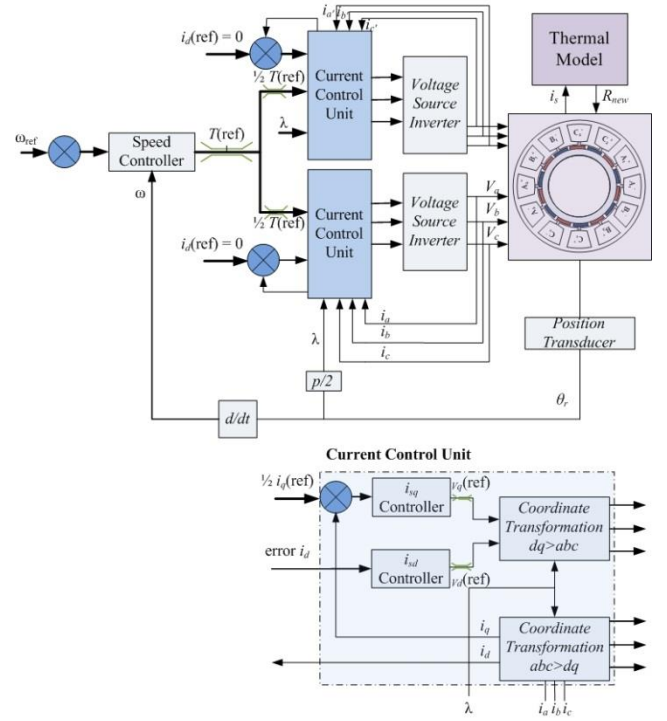

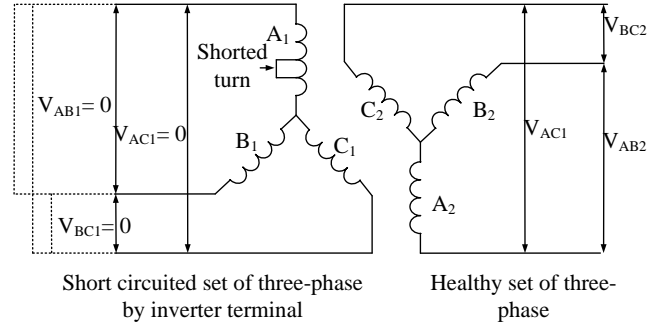Fig.4. Block diagram of the FT-PMSM drive system

Fig.5. Illustration of post-fault control stagey

TABLE I
SPECIFICATION OF THE SIX PHASE FT - PMSM

Rated Speed	2000 rpm
Rated Output Power	2070 W
Rated Current *(Peak)*	10 A
Back-emf *(Peak)*	64.5 V
Phase Resistance	0.22529 Ω
Phase Inductance	0.0043 H
Slot height*(hs)*	12.5 mm
Air gap Length (includes *hm*)	4 mm
Slot Opening *(bo)*	1.65 mm
Tooth Shoe height *(ht)*	2 mm
Slot Wedge	1 mm
Outer Rotor Radius	27.5 mm
Resistivity coefficient of copper	0.004 °C^{-1}
Specific thermal heat capacity of the copper	385 J.kg^{-1}C^{-1}

IV. CONTROL ENVIRONMENT

A standard vector control algorithm [34] is adopted. The d-component of current is always controlled to zero based on the assumption of no field weakening requirement and a non-salient machine. Fig.4 shows the block diagram of the implemented speed controlled system. The machine winding is arranged to be a dual 3-phase configuration.

As explained beforehand the fault-tolerant control strategy is based on applying a balanced 3-phase short-circuit to the winding set which experiences a failure as shown in Fig.5. The torque is produced by both machines under healthy operation. As soon as a fault is detected [7], the post-fault control (i.e. shorting set of three-phase of faulty machine) is applied. Consequently the SC current in the shorted turn reduces and the torque ripple increases slightly than healthy operation. However the torque ripple and unbalance radial forces in faulty operating condition are less than the separated multi-phase approach [18] due to low pulsation; consequently less breaking torque. In addition to the load torque, the breaking torque generated in the faulty machine is also compensated by the healthy machine.

TABLE II
CALCULATED INDUCTANCES FOR VSW

POSITION OF A TURN FAULT	L_s (uH)	L_h (mH)	L_m (uH)
1	1.1225	4.2589	68.5602
13	1.0779	4.2592	68.3348
26	1.0344	4.2601	67.6120
33	1.0236	4.2613	67.3651
39	1.0413	4.2598	67.7485
52	1.0785	4.2591	68.3575
65	1.1236	4.2588	68.5961
5 turns fault	29.6144	3.9055	330.0266
10 turns fault	117.1189	3.2746	601.7664
15 turns fault	260.5958	2.7016	816.5675

V. SIMULATED BEHAVIOR OF THE DRIVE SYSTEM UNDER INTER-TURN SC FAULTS

The specifications of the 12-slot/14-pole dual three-phase machine utilized in this analysis are given in the Table I. Each phase winding has 65 turns which are wound concentrically around a slot using VSW as shown in Fig.6.
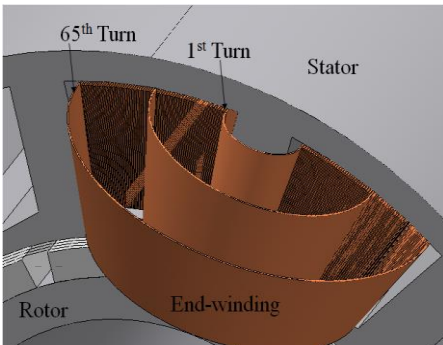

Fig.6. Perspective view of the VSW

Since a single turn SC is the worst case scenario [35], simulations are done for this condition for different fault locations which correspond to the position in the slot of a shorted turn whose number is 1, 13, 26, 33, 39, 52 and 65 respectively (1 being the innermost turn with the lowest resistance whilst 65 is the outermost turn with the highest resistance). The position dependent inductances; self-inductances of the shorted turns (L_s) and the remaining healthy turns (L_h), and mutual inductance (L_m) between them, which are calculated in [6], are given in Table II. The behavior of the machine under healthy, faulty and post fault control stage is investigated. To validate the modeling method adopted fully coupled FE simulations were also undertaken and the results are compared in the following figures.

a – inter-turn SC fault
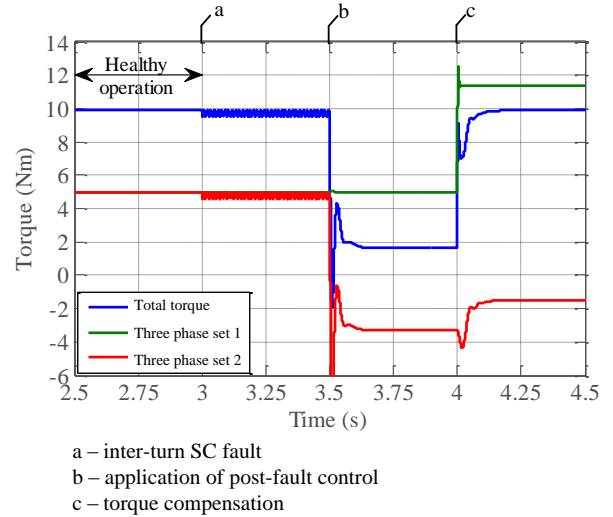b – application of post-fault control
c – torque compensation

Fig.7. Torque behavior under healthy, fault and post-fault control conditions

Fig.7 shows torque behaviour of the drive under healthy, faulty and post-fault control operating conditions. Note that the machine is vector-controlled without speed regulation. The worst case inter-turn SC fault is introduced at t = 3s followed by remedial action at t = 3.5s. Finally torque is compensated at t = 4s by loading the healthy 3-phase set. The obtained result shows a significant torque ripple during faulty condition. It can be seen that this torque ripple decreases drastically when the post-fault control is applied. The resultant torque is dropped by 80% due to reduction in torque contribution of one three-phase set as well as due to the additional breaking torque corresponding to the losses in the short-circuited machine. Normal operation is restored by increasing the load current of the healthy machine by a slightly higher value than twice the original value (10 A) of the rated current (22.45 A). This is partly due to the machine needing to overcome the breaking torque produced by the faulty unit and partly due to the decreasing torque constant with current due to saturation. Such a machine needs to be designed to handle the additional current loading in accordance with the post-fault operating requirements [18, 36]. Fig.8a and b show the computed transient and steady state SC current compared to FE before and after the application of the remedial action (*i.e.* applying a terminal SC), respectively; as can be observed the results are in good agreement.
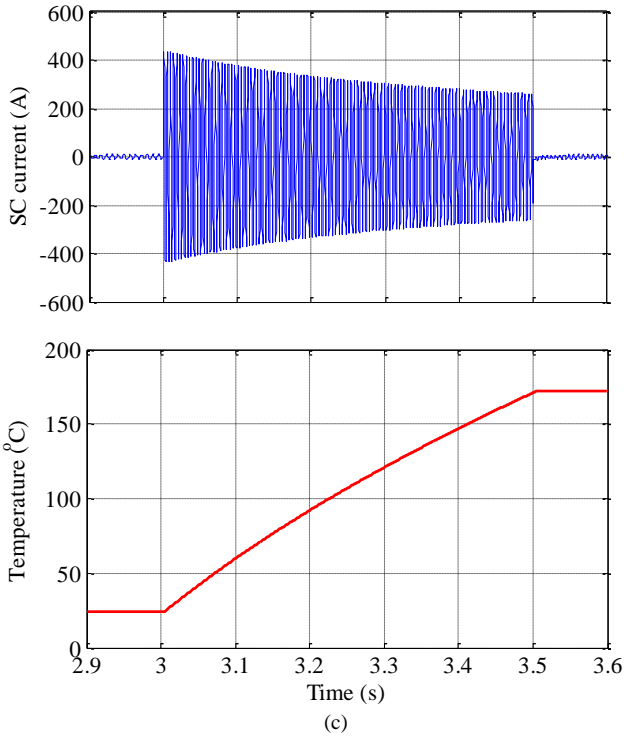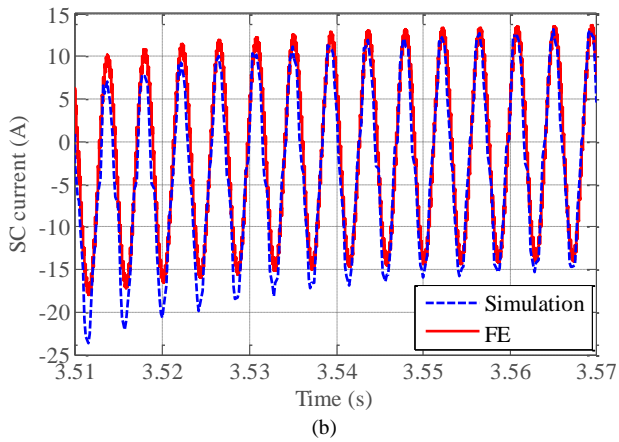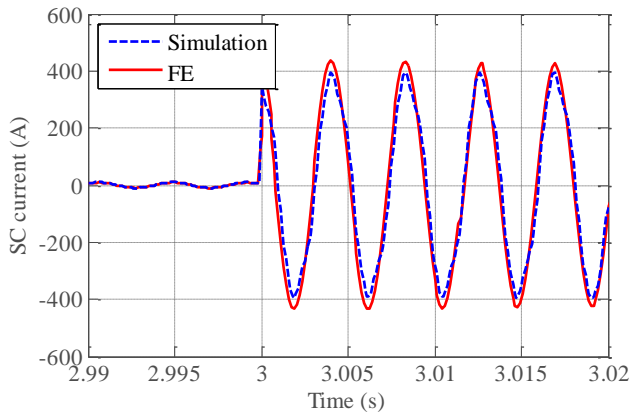
Fig.8c shows the temperature excursion in the shorted turn during the three operating conditions, i.e. healthy, faulty and post-fault remedial control. The result obtained shows a very high current induced in the shorted turn which decreases with increasing resistance due to a rapid temperature rise. From the results above, it is clear that it is only possible to operate the machine for a very short time following a fault occurrence before inducing further failure. A diagnostic algorithm able to detect such a failure mode would be required to initiate the remedial control strategy before further failure is induced.
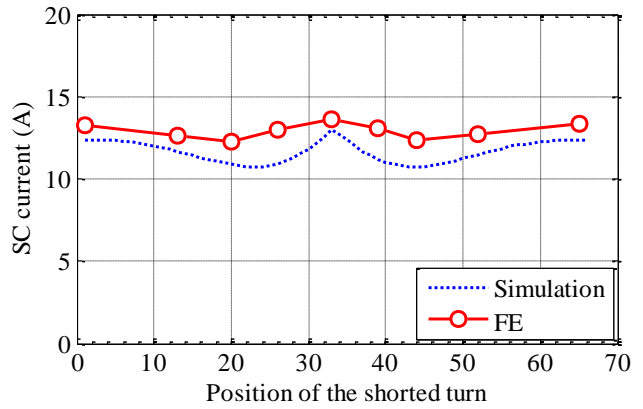

Fig.9. Steady-state current in the shorted turn after application of the remedial action vs. fault location
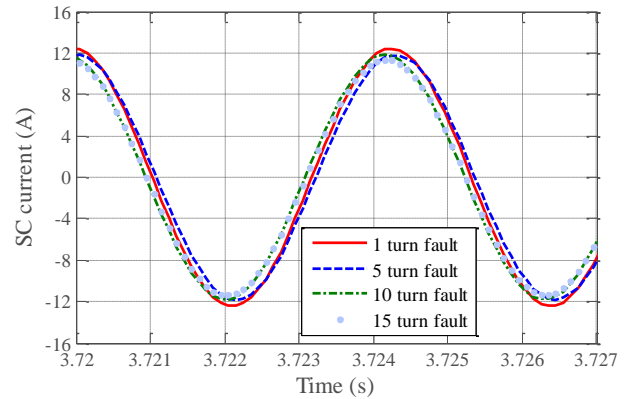

Fig.10. Steady-state current in the different turns SC fault

Fig.8. Transient current in the shorted turn: (a) before, (b) after application of the remedial action. (c). behavior of the 1) fault current, 2) temperature differential in the shorted turn at steady state, faulty and post-fault control conditions

Fig.9 shows the inter-turn SC fault current against the position of the fault (as indicated in Fig.6) in the slot. Obtained SC current for different number of shorted turns is also given in Fig.10. From Fig. 9, it can be seen that the steady-state SC current reaches its maximum value when the fault is located in the middle of the slot. It is important to note that the induced current in the shorted turn of the VSW is almost constant whatever the position in the slot and the number of shorted turns. However, it is not the case for RCW, where significantly large SC current is induced for a single turn fault [6]. This is further explained in the next section.
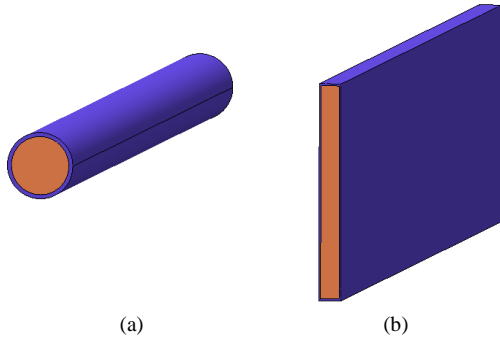
Fig.11. Cross section view of (a) RCW and (b) VSW

VI. COMPARISON WITH CONVENTIONAL ROUND CONDUCTORS WINDING

In order to evaluate the effectiveness of the proposed VSW is compared to a conventional RCW. For the sake of clarity, the cross section views of both winding configurations are given in Fig.11.

The same modeling methodology described in Section III was adopted for both concepts with the equivalent circuit parameters for the round conductors winding calculated as in [6]. The following aspects are compared:

A. *Inter-turn SC current limiting capability*
B. *Copper Losses*
C. *Thermal behavior*

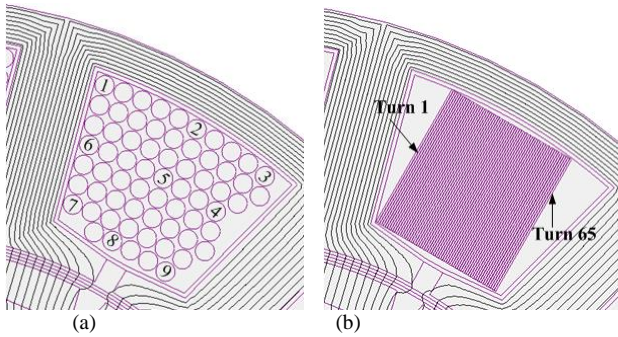Fig.12. Representation of the short-circuit fault location of the (a) RCW (b) VSW

1) *Inter-turn short-circuit current limiting capability*

The SC current in the RCW is computed assuming that the fault is located at various positions within the slot of the same FT-PMSM machine described beforehand and as shown in Fig.12a. Obtained steady-state SC current of RCW (for the numbered fault location indicated in Fig.12a) is given in Fig.13. The turn-turn SC current of a corresponding VSW for a number of fault positions along the coil as illustrated in Fig.12b, are also given in Fig 13. From the results, it can be seen that the induced current in the RCW reaches over four times the rated current when the fault is located in the bottom

of the slot. This result shows clearly that the VSW, as opposed to a conventional winding, intrinsically limits the SC current.
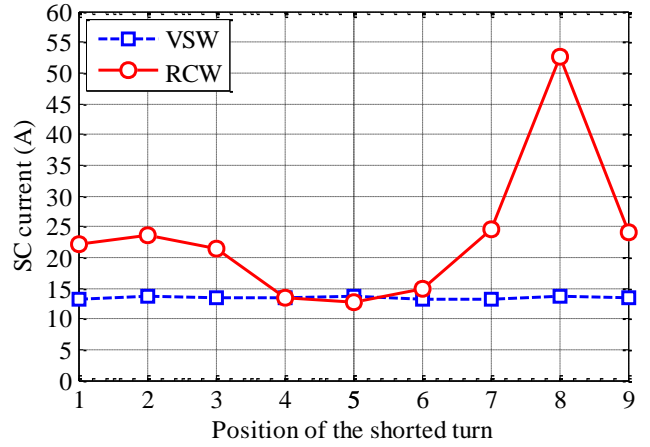

Fig.13. Short-circuit current vs. shorted turn position. Comparison between vertical and round-conductor windings

2) *Copper Losses*

The winding copper loss which influences directly efficiency, or indirectly torque and power density can increase significantly when adopting vertically placed conductors due to eddy-current effects, particularly at high speed. There are two different phenomena that contribute to the total eddy-current effect: skin effect and proximity effect which is also named as double sided skin effect [37]. The skin effect is the tendency for very high frequency currents to flow in the surface of the conductor and the proximity is the tendency for current to flow in other undesirable patterns that form a localized current distribution in the slot due to the presence of an external field which can be produced by either the magnets or adjacent surrounding conductors [38, 39]. The effects are dependent on the physical structure of winding, conductor's length, slot dimensions and operating frequency.
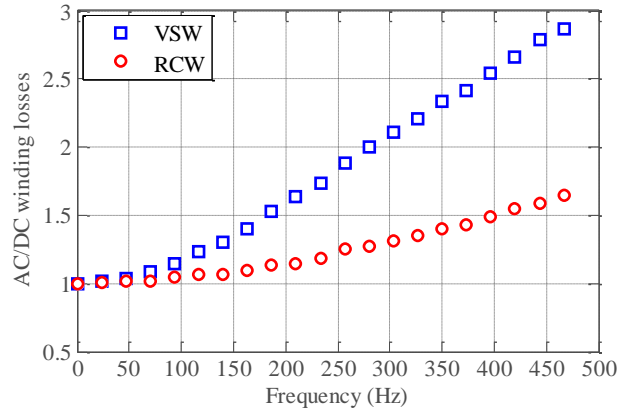

Fig.14. AC/DC Loss ratio vs. frequency. Comparison between VSW and RCW

In order to evaluate the copper loss an assumption is made that there are no changes in the effective resistance due to the temperature rise. The same FT-PMSM is considered for both winding configurations and both conductors have the same cross sectional area (thus, equal DC resistance).

Fig.14 shows the ratio of AC (sum of DC eddy-current loss) to DC loss against frequency. As can be seen, the two winding configurations have the same AC loss at low frequency while at rated frequency the loss of the VSW is twice the value of the one of RCW; this is due to the leakage flux being sheared almost equally by all the VSW conductors. This is a disadvantage of this type of winding. However, the VSW is suitable for relatively low frequency applications, where AC losses are not critical. For high frequency applications, design optimization is necessary to balance the AC losses with the resulting SC currents [40].
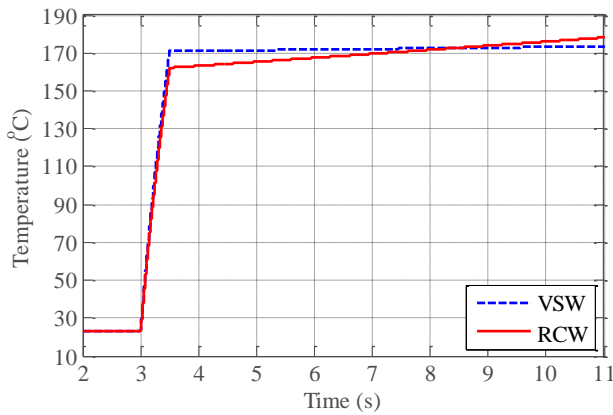

Fig.15. Temperature differential of vertical and stranded windings before and after the remedial action is introduced at 3.5s

3) Thermal behaviour

The temperature rise in the shorted turns was first investigated. As in previous analysis a worst case single turn fault is considered for all the cases to follow. The same FT-PMSM is again considered and the resistance of both windings is assumed to be the same.

As expected, when the fault is applied temperature in the shorted turn increases rapidly as shown in Fig.15. It can be noted that temperature in the VSW increases sharper than in the round conductor winding. This is due to a higher mutual coupling between the faulty and the remaining healthy turns which increase the resulting SC current. However the temperature rise is limited (at t = 3.5s) by the remedial control stagey as soon as the fault is detected [41].

From Fig.15 it can be seen that the temperature differential in the shorted turn of the VSW becomes insignificant after application of the remedial action and thus the machine can be operated safely with the remaining 3-phase set. The SC fault current of the RCW is significantly higher (52A) than the nominal current (10A). As a result the temperature increases further as shown in Fig.15.
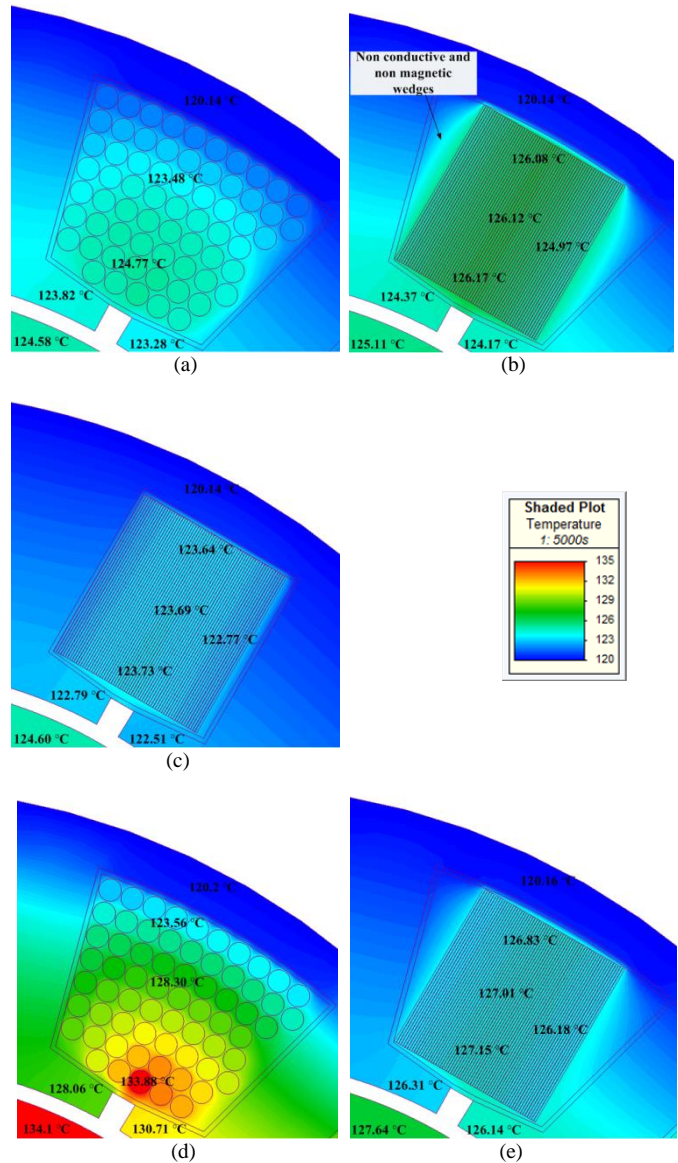

Fig.16. FE temperature distribution of: (a) RCW, (b) VSW, (c) modified slot for VSW at healthy operation and (d) RCW, (e) VSW at faulty operation (after application of the remedial action)

To further investigate the thermal behavior of the proposed winding, 2D FE thermal analysis is carried out to predict the temperature distribution in the slot under both healthy and faulty operation. The study is carried out in a coupled electromagnetic and thermal FE simulation environment [42, 43]. The same FT-PMSM is used in this analysis, where the cross section area, insulation thickness, slot coating, slot dimensions and thermal boundaries (stator outer surface temperature is fixed to 120 °C) are kept the same for both windings. Both windings are designed to have the same fill factor ($K_f = 0.65$).

Fig.16a,b,c and 16d,e show the slot temperature distribution for both windings during healthy operation ($I = 10$ A, $\omega_{rpm}=$ 2000 rpm) and faulty operation (after application of the remedial action), respectively. It can be seen that the VSW hotspot value (126.17°C) is higher than that of RCW (124.77°C). This is expected as the copper losses in the VSW

for the machine adopted in this study are twice the ones of the RCW at rated speed (ω_{rpm} = 2000 rpm).

To overcome this problem, a solution consists to design the slot geometry with respect to the shape of the strip conductors so as to facilitate thermal conduction between the slot and the iron. Fig. 16.c shows the much improved scenario. The main advantage of the VSW in terms of heat transfer is that it has an equivalent winding radial conductivity which is close to that of copper. By doing so the temperature is limited to its equivalent excursion in RCW. The hot spot, which is towards the slot opening, is markedly higher in the stranded winding during faulty conditions, as can be seen in Fig.16.d and e.

In conclusion, from the comparison between VSW and RCW, it can be seen that although the VSW improves fault-tolerant capability, the generated losses in the windings are significantly higher than those of RCW. However these losses can be reduced in the design stage by acting upon the machine geometrical parameters: split ratio, tooth-width/slot pitch ratio and slot opening [40]. Another advantage of the VSW is the fact that it has a better thermal path to the generated copper losses.

TABLE III
SPECIFICATION OF EXPERIMENTED PM MACHINE

Rated speed	2000 rpm	Number of phase	3
Rated torque	6 Nm	Number of slot	18
Output Power	1.25 kW	Number of pole	12
Rated current (rms)	7 A	Phase inductance	5.4 mH
Back-emf (rms)	47.3 V	Phase resistance	125mΩ
Number of turns	40		

VII. EXPERIMENTAL VALIDATION

To assess experimentally the behaviour of the proposed winding, an existing 12-pole/18-slot PM machine wound concentrically with strip conductors was used (specifications of which are given in Table III). Its rotor and stator are shown in Fig.17.
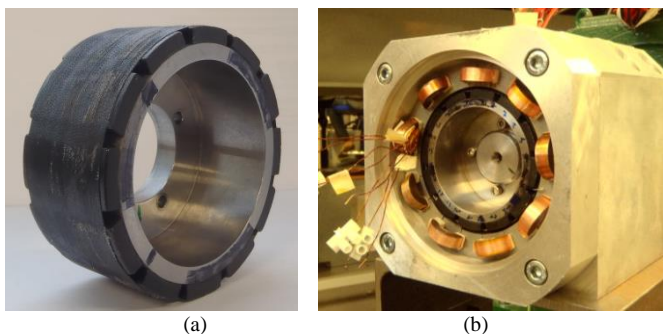

Fig.17. (a) 12 pole rotor and (b) experimental rig

Phase SC current for different numbers of faulted turns and for different positions in the slot of a single turn SC were measured and compared to both the equivalent circuit model and FE results.
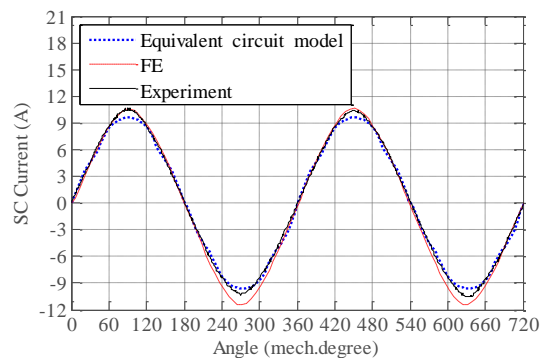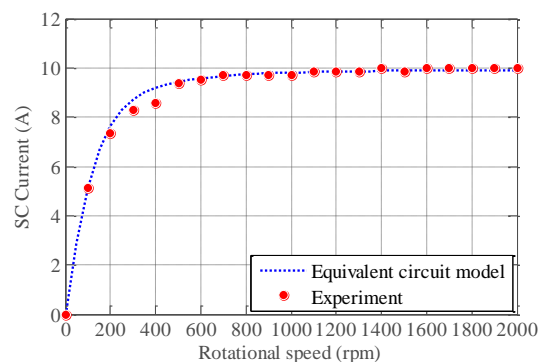

Fig. 18. Phase SC current at 2000 rpm

Fig. 19. Phase SC current vs. rotational speed

As shown in Fig.18, the measured phase SC current is in good agreement with the predicted value. However the magnitude of SC current obtained in the simulation slightly less than the measured ones. This is due to analytically estimated inductance slightly higher than measured and ones calculated in FE [6].

Fig.19 shows the magnitude of the SC current for different rotational speeds under a complete phase SC fault. From the results, it can clearly be seen that the results match the measured ones. Fig.20 compares the inter-turn the measured and calculated SC current after application of the remedial action for a faulted turn located in the middle of the slot. Where, the SC current is calculated considering the impedance of both the end-windings and the external shorting conductors.
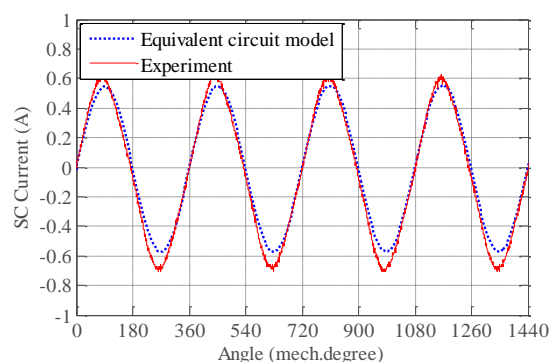

Fig. 20. Inter-turn SC current comparison between simulated and experimented results considering external impedance of shorting connectors.

TABLE IV
COMPARISON OF INTER-TURN SC FAULT CURRENT BETWEEN SIMULATED AND
MEASURED RESULTS AT 2000RPM

Location of the fault	Magnitude of the SC current	
	Simulation	Measured
15th turn	0.593 A	0.602 A
20th turn	0.581 A	0.611 A
35th turn	0.467A	0.472 A

From Fig.20, it can be seen that the estimated results agree with measured ones. From Table IV, it can also be seen that the induced current in a turn is not dependant on the position in the slot of the shorted turn. In reality the SC current slightly reduces with the turn position due to the progressive increase of the end-winding length. These experimental and simulated results confirm that the VSW effectively limits the SC current independently of the position in the slot of the shorted turn.

Fig.21 compares the analytically estimated and measured SC current for different numbers of shorted turn, where the impedance of both the end-winding and the external shorting wires are accounted for. These results are in accordance with predicted ones regardless the number of shorted turns and their position in the slot.
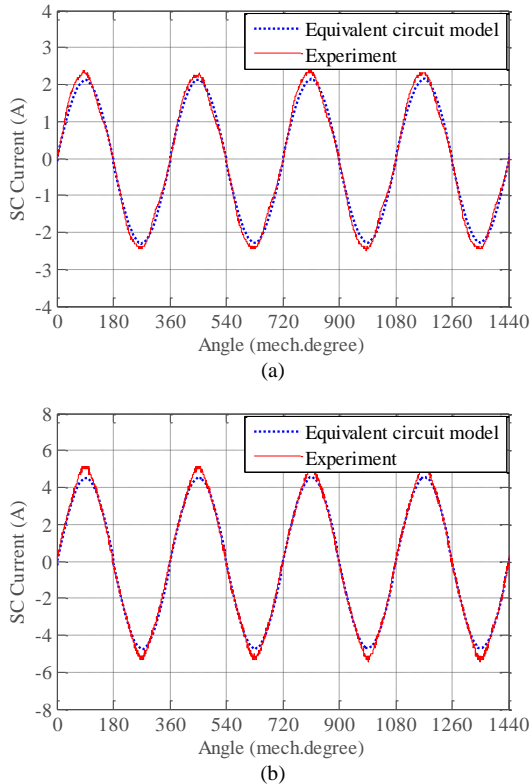

(a)

(b)

Fig.21. Comparison between simulated and experimented results considering external impedance of shorting connectors – (a) 10 turns fault (b) 20turns fault

Fig.22 shows the measured and FE-calculated AC copper loss evolution against the rotational speed. At the rated condition (speed = 2000rpm, current = 7A$_{rms}$) the AC copper loss is 1.5 times higher than the DC loss; It is clear that a

disadvantage of this winding topology is the increased AC copper loss. Design optimization is therefore necessary to balance the AC loss with the resulting SC current when adopting this type of winding, especially for high speed or high pole number applications.
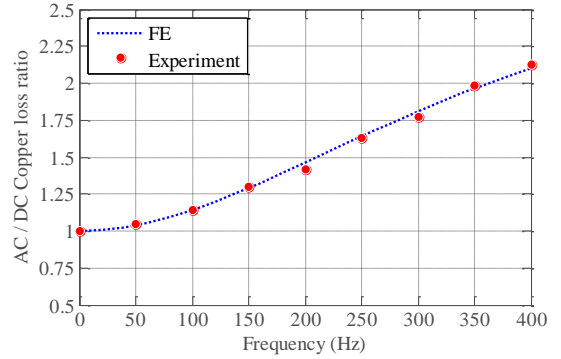

Fig. 22. Total AC/DC winding loss ratio vs. frequency at healthy operating condition
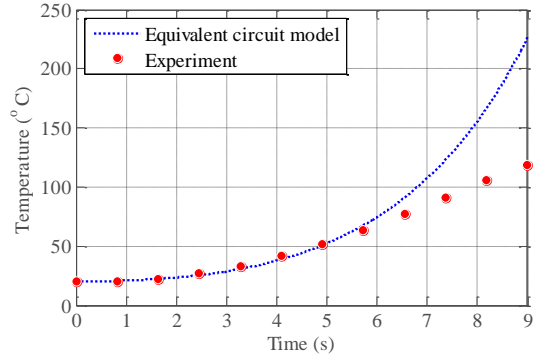

Fig.23. Temperature behavior of a shorted turn under short-circuit fault condition

In order to validate the simplified thermal model adopted the actual temperature rise in a shorted turn under faulty condition was recorded. This time the turn was shorted without using any external leads to have a more representative measurement of a real winding fault. In this case a speed ramp is applied to the machine. The estimated temperature rise in the shorted turn under faulty condition as per the simulation model adopted beforehand is compared to the measured one.

Fig.23 shows that the calculated temperature increase overestimates the measured one after 6 seconds of operation. This is mainly due to the assumption of no heat transfer from the shorted turn to the stator back iron and adjacent conductors. It however validates the assumption of the model representing a worst case condition.

VIII. CONCLUSION

A vertical winding design has been investigated in the context of its fault current limiting capability, losses and thermal behavior. Based on an analytical model that can be used to evaluate inductances and current under SC fault conditions, a dynamic model along with a simplified thermal

model capable of analyzing the dynamic and steady-state behaviors under normal and faulty operation were proposed. The combination of analytical electromagnetic and thermal models facilitates the examination of the faulty behavior. The obtained results have confirmed that the VSW not only improves the fault tolerance capability in terms of inherently limiting the inter-turn SC current but also has a better thermal behavior compared to the RCW; whereas it was shown that there is always a tradeoff between SC current limiting capability and proximity losses. However, the proposed VSW is suitable for relatively low frequency applications, where proximity losses are not critical. For high speed application, design optimization is necessary to balance the AC losses with the resulting SC currents.

REFERENCES

[1] H. Vansompel, P. Sergeant, L. Dupre, and A. Van den Bossche, "Axial flux PM machines with a variable airgap," *Industrial Electronics, IEEE Transactions on,* vol. PP, pp. 1-1, 2013.

[2] K. Kamiev, J. Montonen, M. Ragavendra, J. Pyrhonen, J. Tapia, and M. Niemela, "Design Principles of Permanent Magnet Synchronous Machines for Parallel Hybrid or Traction Applications," *Industrial Electronics, IEEE Transactions on,* vol. PP, pp. 1-1, 2012.

[3] A. Mohammadpour, L. Parsa, and S. Sadeghi, "A Generalized Fault-Tolerant Control Strategy for Five-Phase PM Motor Drives Considering Star, Pentagon and Pentacle Connection of Stator Windings," *Industrial Electronics, IEEE Transactions on,* vol. PP, pp. 1-1, 2013.

[4] A. Sarikhani and O. Mohammed, "Inter-turn Fault Detection in PM Synchronous Machines by Physics-based Back Electromotive Force Estimation," *Industrial Electronics, IEEE Transactions on,* vol. PP, pp. 1-1, 2012.

[5] C. Wenping, B. C. Mecrow, G. J. Atkinson, J. W. Bennett, and D. J. Atkinson, "Overview of Electric Motor Technologies Used for More Electric Aircraft (MEA)," *Industrial Electronics, IEEE Transactions on,* vol. 59, pp. 3523-3531, 2012.

[6] P. Arumugam, T. Hamiti, and C. Gerada, "Modeling of Different Winding Configurations for Fault-Tolerant Permanent Magnet Machines to Restrain Interturn Short-Circuit Current," *Energy Conversion, IEEE Transactions on,* vol. PP, pp. 1-11, 2012.

[7] T. Raminosoa, C. Gerada, and M. Galea, "Design Considerations for a Fault-Tolerant Flux-Switching Permanent-Magnet Machine," *Industrial Electronics, IEEE Transactions on,* vol. 58, pp. 2818-2825, 2011.

[8] M. Barcaro, N. Bianchi, and F. Magnussen, "Faulty Operations of a PM Fractional-Slot Machine With a Dual Three-Phase Winding," *Industrial Electronics, IEEE Transactions on,* vol. 58, pp. 3825-3832, 2011.

[9] S. Dwari and L. Parsa, "Fault-Tolerant Control of Five-Phase Permanent-Magnet Motors With Trapezoidal Back EMF," *Industrial Electronics, IEEE Transactions on,* vol. 58, pp. 476-485, 2011.

[10] S. Zhigang, W. Jiabin, G. W. Jewell, and D. Howe, "Enhanced Optimal Torque Control of Fault-Tolerant PM Machine Under Flux-Weakening Operation," *Industrial Electronics, IEEE Transactions on,* vol. 57, pp. 344-353, 2010.

[11] M. Villani, M. Tursini, G. Fabri, and L. Castellini, "High Reliability Permanent Magnet Brushless Motor Drive for Aircraft Application," *Industrial Electronics, IEEE Transactions on,* vol. 59, pp. 2073-2081, 2012.

[12] H. Xiaoyan, A. Goodman, C. Gerada, F. Youtong, and L. Qinfen, "Design of a Five-Phase Brushless DC Motor for a Safety Critical Aerospace Application," *Industrial Electronics, IEEE Transactions on,* vol. 59, pp. 3532-3541, 2012.

[13] M. Aboelhassan, T. Raminosoa, A. Goodman, L. de Lillo, and C. Gerada, "Performance Evaluation of a Vector Control Fault-Tolerant Flux-Switching Motor Drive," *Industrial Electronics, IEEE Transactions on,* vol. PP, pp. 1-1, 2012.

[14] F. Lin, Y. Hung, and M. Tsai, "Fault Tolerant Control for Six-Phase PMSM Drive System via Intelligent Complementary Sliding Mode Control Using TSKFNN-AMF," *Industrial Electronics, IEEE Transactions on,* vol. PP, pp. 1-1, 2013.

[15] N. M. A. Freire, J. O. Estima, and A. J. M. Cardoso, "Open-Circuit Fault Diagnosis in PMSG Drives for Wind Turbine Applications," *Industrial Electronics, IEEE Transactions on,* vol. PP, pp. 1-1, 2012.

[16] E. Strangas, S. Aviyente, S. Zaidi, and J. Neely, "The Effect of Failure Prognosis and Mitigation on the Reliability of Permanent Magnet AC Motor Drives," *Industrial Electronics, IEEE Transactions on,* vol. PP, pp. 1-1, 2012.

[17] P. Potamianos, E. Mitronikas, and A. Safacas, "Open-Circuit Fault Diagnosis for Matrix Converter Drives and Remedial Operation Using Carrier-Based Modulation Methods," *Industrial Electronics, IEEE Transactions on,* vol. PP, pp. 1-1, 2013.

[18] J. A. Haylock, B. C. Mecrow, A. G. Jack, and D. J. Atkinson, "Operation of fault tolerant machines with winding failures," *Energy Conversion, IEEE Transactions on,* vol. 14, pp. 1490-1495, 1999.

[19] L. Alberti and N. Bianchi, "Experimental Tests of Dual Three-Phase Induction Motor Under Faulty Operating Condition," *Industrial Electronics, IEEE Transactions on,* vol. 59, pp. 2041-2048, 2012.

[20] A. J. Mitcham, G. Antonopoulos, and J. J. A. Cullen, "Implications of shorted turn faults in bar wound PM machines," *Electric Power Applications, IEE Proceedings -,* vol. 151, pp. 651-657, 2004.

[21] C. Gerada, K. J. Bradley, M. Sumner, P. Wheeler, S. Pickering, J. Clare, C. Whitley, and G. Towers, "The results do mesh," *Industry Applications Magazine, IEEE,* vol. 13, pp. 62-72, 2007.

[22] K. D. e. al, "Method and apparatus for controlling an electric machine," 7443070, Oct 28, 2008.

[23] G. E. Horst, "Flux controlled permanent magnet dynamo-electric " 5530307, Mar 28, 1994.

[24] J. Arellano-Padilla, M. Sumner, and C. Gerada, "Winding condition monitoring schemefor a permanent magnet machine using high-frequency injection," *Electric Power Applications, IET,* vol. 5, pp. 89-99, 2011.

[25] M. R. Shah, A. M. El-Refaie, and K. Sivasubramaniam, "Analysis of turn-to-turn faults in surface PM machines with multi-layer fractional-slot concentrated windings," in *Electrical Machines, 2008. ICEM 2008. 18th International Conference on*, 2008, pp. 1-4.

[26] B. Vaseghi, B. Nahid-Mobarakeh, N. Takorabet, and F. Meibody-Tabar, "Experimentally Validated Dynamic Fault Model for PMSM with Stator Winding Inter-Turn Fault," in *Industry Applications Society Annual Meeting, 2008. IAS '08. IEEE*, 2008, pp. 1-5.

[27] A. Gandhi, T. Corrigan, and L. Parsa, "Recent Advances in Modeling and Online Detection of Stator Interturn Faults in Electrical Motors," *Industrial Electronics, IEEE Transactions on,* vol. 58, pp. 1564-1575, 2011.

[28] C. Gerada, K. Bradley, and M. Summer, "Winding turn-to-turn faults in permanent magnet synchronous machine drives," in *Industry Applications Conference, 2005. Fourtieth IAS Annual Meeting. Conference Record of the 2005*, 2005, pp. 1029-1036 Vol. 2.

[29] L. de Lillo, L. Empringham, P. W. Wheeler, S. Khwan-On, C. Gerada, M. N. Othman, and H. Xiaoyan, "Multiphase Power Converter Drive for Fault-Tolerant Machine Development in Aerospace Applications," *Industrial Electronics, IEEE Transactions on,* vol. 57, pp. 575-583, 2010.

[30] A. Akrad, M. Hilairet, and D. Diallo, "Design of a Fault-Tolerant Controller Based on Observers for a PMSM Drive," *Industrial Electronics, IEEE Transactions on,* vol. 58, pp. 1416-1427, 2011.

[31] Z. Meiyang and G. Hui, "Integrative simulation and analysis of induction motor and control system," in *Electronic and Mechanical Engineering and Information Technology (EMEIT), 2011 International Conference on*, 2011, pp. 2412-2414.

[32] B. Vaseghi, N. Takorabet, J. P. Caron, B. Nahid-Mobarakeh, F. Meibody-Tabar, and G. Humbert, "Study of Different Architectures of Fault-Tolerant Actuator Using a Two-Channel PM Motor," *Industry Applications, IEEE Transactions on,* vol. 47, pp. 47-54, 2011.

[33] G. C. Stone, E. A. Boulter, I. Culbert, and H. Dhirani, "Electrical Insulation for Rotating Machines - Design, Evaluation, Aging, Testing and Repair," ed: Wiley - IEEE Press.

[34] A. M. da Silva, R. J. Povinelli, and N. A. O. Demerdash, "Induction Machine Broken Bar and Stator Short-Circuit Fault Diagnostics Based on Three-Phase Stator Current Envelopes," *Industrial Electronics, IEEE Transactions on,* vol. 55, pp. 1310-1318, 2008.

[35] P. Arumugam, T. Hamiti, and C. Gerada, "Analytical modeling of a vertically distributed winding configuration for Fault Tolerant Permanent Magnet Machines to suppress inter-turn short circuit current limiting," in *Electric Machines & Drives Conference (IEMDC), 2011 IEEE International*, 2011, pp. 371-376.

[36] S. Bolognani, M. Zordan, and M. Zigliotto, "Experimental fault-tolerant control of a PMSM drive," *Industrial Electronics, IEEE Transactions on,* vol. 47, pp. 1134-1141, 2000.

[37] J. Pyrhönen, T. Jokinen, and V. Hrabovcová, *Design of rotating electrical machines*: Wiley, 2008.

[38] P. H. Mellor, R. Wrobel, and N. McNeill, "Investigation of Proximity Losses in a High Speed Brushless Permanent Magnet Motor," in *Industry Applications Conference, 2006. 41st IAS Annual Meeting. Conference Record of the 2006 IEEE*, 2006, pp. 1514-1518.

[39] A. Boglietti, A. Cavagnino, and M. Lazzari, "Computational Algorithms for Induction Motor Equivalent Circuit Parameter Determination;Part II: Skin Effect and Magnetizing Characteristics," *Industrial Electronics, IEEE Transactions on,* vol. 58, pp. 3734-3740, 2011.

[40] P. Arumugam, T. Hamiti, and C. Gerada, "Fault tolerant winding design; A compromise between losses and fault tolerant capability," in *Electrical Machines (ICEM), 2012 XXth International Conference on*, 2012, pp. 2559-2565.

[41] G. M. Joksimovic and J. Penman, "The detection of inter-turn short circuits in the stator windings of operating motors," *Industrial Electronics, IEEE Transactions on,* vol. 47, pp. 1078-1084, 2000.

[42] A. Boglietti, A. Cavagnino, D. Staton, M. Shanel, M. Mueller, and C. Mejuto, "Evolution and Modern Approaches for Thermal Analysis of Electrical Machines," *Industrial Electronics, IEEE Transactions on,* vol. 56, pp. 871-882, 2009.

[43] T. Sawata and D. Staton, "Thermal modeling of a short-duty motor," in *IECON 2011 - 37th Annual Conference on IEEE Industrial Electronics Society*, 2011, pp. 2054-2059.

Christopher Brunson received the M.Eng (Hons) degree in Electrical Engineering from the University of Nottingham, U.K, in 2009 and I currently working towards his Ph.D. in Matrix Converter Fault Diagnosis, with the Power Electronics, Machines, and Control Group at the University of Nottingham, Nottingham, U.K. His main research fields are Matrix Converters, and Fault Diagnosis.

Chris Gerada (M'05) obtained his PhD in Numerical Modeling of Electrical Machines from the University of Nottingham, UK in 2005. He subsequently worked as a researcher at the University of Nottingham on high performance electrical drives and on the design and modeling of electromagnetic actuators for aerospace applications. He was appointed as Lecturer in Electrical Machines in 2008, an Associate Professor in 2011 and Professor in 2013. His core research interests include the design and modeling of high performance electric drives and machines. Dr. Gerada has been the project manager of the GE Aviation Strategic Partnership since 2006 and in 2011 was awarded a Royal Academy of Engineering Senior Research Fellowship supported by Cummins. He is also an Associate Editor for the Transactions in Industry Applications and executive member of the management board of the UK Magnetic Society and the IET Aerospace Technical and Professional Network.

Puvan Arumugam received the B.Eng (Hons) degree in electrical and electronic engineering from the University of Nottingham, Nottingham, U.K, in 2009. He is currently working toward the Ph.D. degree in fault tolerant machine design with the Power Electronics, Machines, and Control Group at the University of Nottingham, Nottingham, U.K.

His main research interests are analytical computation of electromagnetic fields in electrical machines and fault tolerant machines.

Tahar Hamiti was born in Larbàa Nath Irathen, Algeria, in 1979. He obtained his Ingénieur d'Etat degree in automatic control systems from the University of Tizi-ouzou, Algeria and the Ph.D. degree in electrical engineering from the University of Nancy I, Nancy, France. From 2010 to 2011 his was a Research Fellow in the Power Electronics, Machines and Control group, University of Nottingham, where he is currently a lecturer. His research interests include modeling, optimal design and control of high performance electrical machines for transportation applications and power generation.